Acta Biomaterialia 9 (2013) 5305–5312

Contents lists available at SciVerse ScienceDirect

Acta Biomaterialia

journal homepage: www.elsevier.com/locate/actabiomat

Effect of X-ray irradiation on the elastic strain evolution in the mineral phase of bovine bone under creep and load-free conditions ☆

Alix C. Deymier-Black [a,*], Anjali Singhal [a], Jonathan D. Almer [b], David C. Dunand [a]

[a] Department of Materials Science and Engineering, Northwestern University, Evanston, IL 60208, USA
[b] X-ray Science Division, Advanced Photon Source, Argonne National Laboratory, Argonne, IL 60439, USA

ARTICLE INFO

Article history:
Available online 5 August 2012

Keywords:
Bone
Synchrotron X-ray diffraction
Creep
Radiation damage
Residual strain

ABSTRACT

Both the load partitioning between hydroxyapatite (HAP) and collagen during compressive creep deformation of bone and the HAP residual strain in unloaded bone have been shown in previous synchrotron X-ray diffraction studies to be affected by the X-ray irradiation dose. Here, through detailed analysis of the X-ray diffraction patterns of bovine bone, the effect of X-ray dose on (i) the rate of HAP elastic strain accumulation/shedding under creep conditions and (ii) the HAP lattice spacing and average root mean square (RMS) strain under load-free conditions are examined. These strain measurements exhibit three stages in response to increasing X-ray dose. Up to ~75 kGy (stage I) no effect of dose is observed, indicating a threshold behavior. Between ~75 and ~300 kGy (stage II) in unloaded bone the HAP *d*-spacing increases and the RMS strain decreases with dose, indicating strain relaxation of HAP. Furthermore, under constant compressive load creep conditions, the rate of compressive elastic strain accumulation in HAP decreases with increasing dose until, at ~115 kGy, it changes sign, indicating that the HAP phase is shedding load during creep deformation. These stage II behaviors are consistent with HAP–collagen interfacial damage, which allows the HAP elastic strain to relax within both the loaded and unloaded samples. Finally, for doses in excess of ~300 kGy (stage III, measured up to 7771 kGy) the HAP lattice spacing and RMS strain for load-free samples and the rate of HAP elastic strain shedding for crept samples remain independent of dose, suggesting a saturation of damage and/or stiffening of the collagen matrix due to intermolecular cross-linking.

1. Introduction

Compact bone is a complex hierarchical composite composed of two solid phases, a mineral phase (hydroxyapatite, HAP) and a proteinaceous phase (mostly type 1 collagen), with pores containing fluid (water, blood, or biological serum). The properties of the two solid phases, as well as their structural organization and bonding, explain the unusual combination of high toughness and high strength of bone [1–4]. Variation in the properties of HAP, protein, or their interfaces can cause changes in the macroscopic properties of the bone. For example, irradiation, which can affect the collagen and its interfacial bonding with HAP, affects the mechanical properties of cortical bone [5–10], as summarized later.

Bones can be exposed to varying doses of ionizing radiation for an assortment of reasons. Low doses of radiation can be accumulated from medical X-rays (~0.03 Gy), extended space travel (~2 Gy) [11,12], or radiation cancer treatments (7–60 Gy) [13–15]. Higher doses, 17–100 kGy, are used to sterilize bone allografts limiting the spread of bacteria and viruses after implantation [16,17]. Currently ex vivo synchrotron X-ray experiments on bone, both tomographic imaging and strain measurements, lead to even higher X-ray irradiation doses of the order of hundreds to thousands of kilograys [18–27]. The importance of radiation treatments and basic biomaterials research in medical science has made understanding the effects of such radiation on bone mechanics essential.

Many studies have shown that ionizing radiation can have significant effects on the mechanical behavior of bone. While bone stiffness and hardness are not significantly affected by doses in the sterilization range [8,10,28], post-yield properties (e.g. fracture toughness, work to failure, fatigue failure impact energy absorption, ultimate strength, and bending strength) are significantly reduced after irradiation doses of 17–100 kGy [5,7,8,29]. This has been attributed to cross-linking or denaturation of the collagen phase. However, these studies only examined the macroscopic behaviors of bone, making it difficult to establish clear conclusions about how the individual phases (HAP and collagen) and their interface are affected by irradiation.

☆ Part of the Special Issue "TMS 2012 Biological Materials", guest-edited by Professor Nima Rahbar.

* Corresponding author. Current address: Dept. of Othropaedic Surgery, Washington University at Saint Louis School of Medicine St Louis, MO 63110,USA. Tel.: +314 747 6265; fax: +314 454 5900.
E-mail address: a.black@wustl.edu (A.C. Deymier-Black).

1742-7061/$ - see front matter © 2012 Acta Materialia Inc. Published by Elsevier Ltd. All rights reserved.
http://dx.doi.org/10.1016/j.actbio.2012.07.046

Recent studies using high energy synchrotron X-ray diffraction have provided insights into how the HAP platelets and mineralized collagen fibrils behave mechanically within irradiated bone on the nanometer scale. This technique has previously been used to study the load transfer behavior between the phases (HAP and collagen) of antlers, bones, and teeth [18–25,30–33]. The latest studies have focused on the effects of irradiation on the elastic and creep behaviors of bone [6,9,10]. Published data show that with irradiation doses up to 3840 kGy load transfer between the collagen and HAP during elastic loading does not change within experimental error [6,10]. However, there is a significant decrease in the HAP residual strain with increased dose [10]. In irradiated bone samples under load HAP strains produced initially during elastic loading also decrease with creep time (i.e. HAP sheds some of its elastic load during creep deformation) [9], which is the opposite of the behavior measured in unirradiated bone [33]. It has been suggested that this HAP load shedding, visible during creep and after unloading, is due to collagen damage, especially at the carboxyl side-chains, leading to increased HAP/collagen interfacial damage [9,10,34].

Accordingly, HAP/collagen interfacial damage (which may result from decarboxylation of the collagen side-chains decreasing the number of ion-mediated bonds between the two phases [34]) results in a weakened interface and thus reduces the ability of collagen to transfer load to HAP under an applied load, and promotes relaxation of HAP residual strain when unloaded. Although these studies have given a greater understanding of the effects of high energy X-ray irradiation on the mechanical interaction between HAP and collagen in bone, it is important to investigate in greater detail the doses at which the mechanical properties of bone become compromised.

In the present study high energy X-ray diffraction was used to examine the effect of X-ray irradiation on the HAP strain in bone, under both mechanically loaded and unloaded conditions.

2. Experimental procedures

2.1. Sample preparation

Fresh bovine femurs of a healthy 18-month-old Black Angus cow were obtained from a local abattoir (Aurora Packing Co. Inc., North Aurora, IL) within 1 h after slaughter. The femurs were cleaned of marrow and any attached ligaments were removed using scalpels. Two nearly cylindrical sections (proximal and distal) were created from each femur by making cuts with a Stryker 810 autopsy saw (Stryker, Mahwah, NJ) perpendicular to their longitudinal axis, approximately 6 cm apart, and frozen in gauze soaked in phosphate-buffered saline (PBS) at −25 °C until further cutting. At a later date the sections were thawed to room temperature and, using a low speed diamond saw, parallel cuts were made along the transverse axis of the cylindrical regions approximately 5.5 mm apart. Further cuts were made within the plane of these transverse sections to produce pure cortical bone samples with approximate dimensions $5 \times 4 \times 3$ mm. The samples were obtained from the anterio-medial and anterio-lateral regions of a single femur cross-section. After cutting the samples were blotted dry and weighed with a precision balance and their dimensions measured with a point micrometer, taking each measurement three times. These samples were stored in PBS and frozen at −20 °C until the time of the experiment.

2.2. Diffraction experiments

2.2.1. Irradiation without load

All the tests were performed in beamline 1-ID of the Advanced Photon Source (APS), Argonne National Laboratory (Argonne, IL). Three samples were thawed to room temperature prior to testing. The samples were placed in a custom designed hydration container made of lexan. The container holds three samples with the aforementioned dimensions, with a spacing of 2.5 mm between adjacent samples. The samples were placed in the container such that their 3 mm dimension was traversed by the X-ray beam. The temperature of the solution in the sample container was maintained at 37 °C, near the bovine body temperature of 37.8–39.4 °C, throughout the experiment by the continuous flow of temperature controlled PBS heated in an external water bath. The set-up for the experiment is shown in Fig. 1. A total of six samples were studied as two sets of three samples each. The left-most samples in sets 1 and 2 served as controls (termed LC1 and LC2) and were not irradiated. The middle (labeled M1 and M2) and the right-most samples (labeled R1 and R2) were irradiated to maximum doses of 3800 kGy. For each sample diffraction measurements were carried out at three locations, the horizontal center and 250 μm to either side, before they were subjected to any

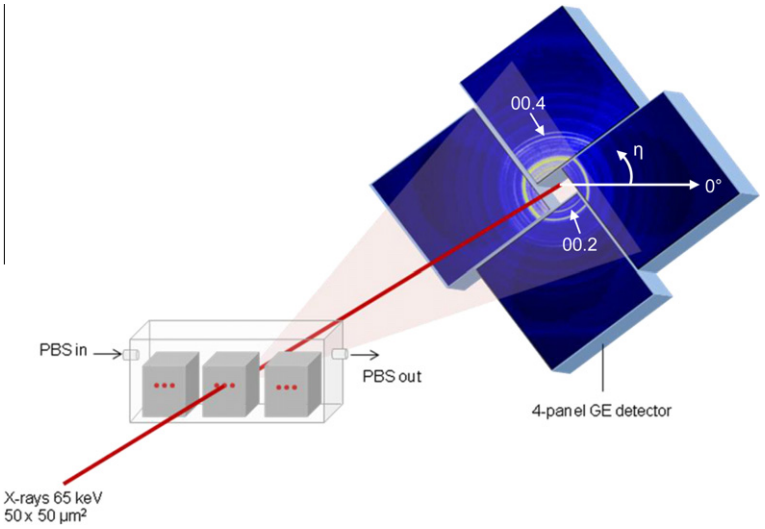

Fig. 1. Experimental set-up for the experiments without load performed on irradiated samples M1–2 and R1–2 and control samples LC1 and LC2. The diffraction rings shown on the detectors are for sample LC1. Image not to scale.

additional irradiation. The measurements were done with a 50 × 50 μm X-ray beam of 65 keV (wavelength 0.19 Å) energy using a 2 s exposure time. The radiation dose absorbed by the samples during each of these 2 s measurements was 0.7 kGy. The diffraction patterns were collected on a wide-angle X-ray scattering (WAXS) detector, placed at a distance of 1994 mm from the sample. As shown in Fig. 1, the detector consisted of four GE-41RT flat panel detectors (2048 × 2048 pixels, 200 × 200 μm per pixel) arranged in a flower-shaped pattern to avoid the transmitted beam; each detector was rotated in an anticlockwise direction at an angle of 37° with respect to its horizontal direction. The detectors were calibrated with a pressed ceria powder disc (CeO_2, NIST SRM-674a) at the beginning and end of the experimentation time. After the initial measurement samples M1–2 and R1–2 were irradiated using a wide X-ray beam of 3 × 0.2 mm size. The X-ray beam had a Gaussian flux profile, arising from the undulator characteristics, with a full width at half maximum (FWHM) of 1.4 mm. The samples were exposed to the X-rays for a predetermined amount of time to accumulate the required dose level. Thereafter, the size of the X-ray beam was reduced to that used for diffraction measurements (50 × 50 μm); measurements were performed at the same three locations as the initial ones. This process of irradiation/measurement was repeated until a total dose of 3800 kGy was accumulated by each of the samples.

The control samples (LC1 and LC2) were not subjected to any wide beam irradiation but were measured at the same time intervals as the irradiated samples. The total irradiation dose for the control samples as a result of the measurements was 4.9 kGy, a dose at which the mechanical properties of bone are not expected to be significantly altered [5,10,33].

2.2.2. Irradiation under load

For the irradiation under load experiments a single sample at a time was placed on the lower platen of a servo-hydraulic MTS-858 load frame. A hydration rig made of vinyl tubing was attached to the lower platen to keep the sample hydrated, as described previously [10,32]. Temperature controlled PBS was flowed through the sample container to maintain the solution at a temperature of 37 °C. The samples were loaded in compression to −80 MPa along the longitudinal axis of the femur samples, and a beam of 70 keV (wavelength 0.18 Å) X-rays was directed perpendicular to the loading direction and at the center of the sample. The samples were irradiated to different dose levels, 7771 kGy being the highest dose, over an area of 3 × 0.2 mm, similarly to the set of experiments described in Section 2.2.1. Following this irradiation a single wide angle scattering measurement was carried out near the center of the sample. Scattering measurements were begun immediately following application of the −80 MPa stress so that the initial elastic strain could be recorded. To minimize the accumulated radiation damage from measurements at a single spot the scattering measurements were spread over an array of 20 points in two rows of 10 points each. These diffraction measurements are carried out using the same pattern as described in our previous work. [33]. The 10 points in each row were chosen to be located about the horizontal and vertical center of the sample. The two rows were spaced 100 μm apart vertically; horizontally neighboring points were also spaced 100 μm apart. The measurements were started at the top left-most location, proceeding towards the right, and then moving to the bottom row, also measuring from left to right. To obtain data for a period of two hours, the array was measured four times. The samples were exposed to the X-rays for 1 s to obtain diffraction measurements. A 50 × 50 μm X-ray beam of 70 keV energy was used and the dose absorbed by the sample was 0.15 kGy s^{-1}. The diffraction patterns were collected by a single GE-RT41 detector centered on the direct beam at a distance of 1137 mm from the sample. The detector was calibrated using a pressed ceria powder disc as described in Section 2.2.1.

Five other samples, labeled A1, A2, H1, I1 and I2, which were run during a separate experiment than those described above or in Section 2.2.1, were also included in this study. All other parameters (measurement routine, number of measurement points, and detector) being the same, these samples were measured with X-rays of 65 keV energy and a vertically focused beam which resulted in an absorbed dose of 0.6 kGy s^{-1} by the sample. Samples A1 and A2 are described in Deymier-Black et al. [33].

2.3. Diffraction analysis

2.3.1. HAP peak broadening analysis

The diffraction data analysis was performed as described previously in the literature [10,20]. The ceria diffraction pattern was used to calculate accurate values of sample to detector distance, detector tilt, and detector rotation for each detector using the software FIT2D [35]. These parameters were then fed into a series of algorithms custom written in MATLAB (Mathworks, Natick, MA). The program collates the diffraction patterns from the four detectors and transforms them into Cartesian coordinates. Diffraction patterns from bone samples were highly textured, with the HAP *c*-axis being preferentially aligned towards ~110°, as shown in Fig. 1. Since the HAP *c*-axis was preferentially aligned with the long axis of the bone that was nominally aligned with the long axis of the samples, this suggests that the bone samples (LC1–2, M1–2, and R1–2) were cut with a misalignment of ~20° from the sample long axis. In order to investigate the true longitudinal behavior of bone all the strain values extracted from these diffraction data were measured along the axis of highest intensity (110°) and not the expected 90°. To do this the (00.2), (31.0), and (00.4) HAP peak intensities were binned into 10° bins with the first bin being 5 ± 5°. The peak shapes for (00.2) and (00.4) were investigated at 110 ± 5° and 290 ± 5° to obtain longitudinal values of peak broadening. The peaks shapes for (31.0) were investigated at 205 ± 5° and 215 ± 5° to obtain the transverse values of peak broadening. Assuming a Gaussian shape for the diffraction peaks, they were fitted using a pseudo-Voigt function to calculate the peak center.

The peak FWHM determined from these fits is affected by three contributions: instrumental broadening, broadening due to small crystallite sizes and broadening due to inhomogeneous strains within the sampled volume. The instrumental broadening is determined from the diffraction pattern of the ceria standard, which is known to have very little intrinsic sample broadening. The Ce(111) diffraction peak has a peak width of ~3.12 Å. The contributions due to the crystallite size and strain can then be deconvoluted using the (00.2) and (00.4) peaks and the Scherrer equation [36]:

$$\Delta 2\theta \cos\theta = (\lambda/D) + 2\varepsilon_{rms} \sin\theta \quad (1)$$

where $\Delta 2\theta$ is the FWHM of the peak in radians, λ is the X-ray wavelength, θ is the diffraction angle, D is the coherent size of the platelets, and ε_{rms} denotes the root mean square (RMS) strain or the distribution of strains within the volume sampled by the X-ray beam. The coherent size of the platelets D in the transverse direction was evaluated assuming an ε_{rms} value of 0 in Eq. (1).

2.3.2. HAP strain analysis

The radial distance at the peak centers (r_η) of the HAP diffraction patterns were determined for all the azimuths (η) from the centers of the fitted peaks described above. Only the longitudinal *d*-spacings are reported for samples LC1–2, M1–2, and R1–2; they were obtained at 110 ± 5° and 290 ± 5°, i.e. at the locations of highest intensity.

For the samples which underwent creep the HAP strain is calculated using the equation:

$$\varepsilon_\eta = (r^* - r_\eta)/r_\eta \quad (2)$$

Here r^* is the invariant strain radius of the HAP diffraction pattern, which is inversely proportional to the unstrained lattice spacing d_o and is found as the point of intersection of r vs. η responses for a number of applied stresses on the sample. However, in this case of creep, since only a single load is applied, a standard value of r^* (or equivalently d_o) determined from our previous studies on the same type of bovine bone was used in the strain calculations [10,37]. As mentioned earlier, only the longitudinal strains obtained at 90 ± 10° and 270 ± 10° are reported here.

3. Results

3.1. Irradiation without loading

3.1.1. HAP peak FWHM

The azimuthally averaged raw (00.2) diffraction intensity peaks (from 105° to 115°) as a function of d-spacing for a single control (LC1) and irradiated sample (R1) are shown in Fig. 2a and b, where the peak intensity is normalized to the maximum intensity in the diffraction ring. The peak widths under the initial condition (2 kGy) and after doses of 693 and 2935 kGy are shown for the irradiated sample. The peak widths in the control sample are shown at the same times that the irradiated samples were exposed to X-rays (except the value of 0.7 kGy associated with each of the diffraction measurements). Comparison of Fig. 2a and b clearly shows that the peaks from the irradiated sample sharpen with increasing dose from 2 to 2935 kGy, whereas those from the control sample remain unchanged. Fig. 2a also reveals an asymmetric sharpening of the peak whereby the peak width reduces to a greater extent in the region with lower d-spacing values, compared with the high d-spacing region. This asymmetric sharpening of the peak is seen in all the irradiated samples M1, M2, R1, and R2.

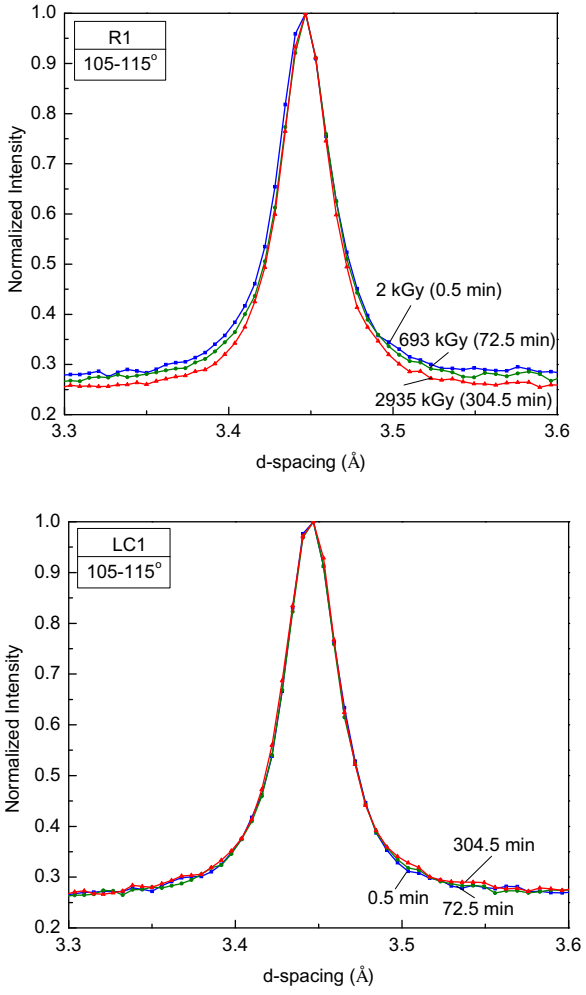

Fig. 2. Normalized X-ray diffraction intensity as a function of d-spacing for the longitudinal HAP(00.2) peak azimuthally averaged from 105° to 115° for (a) irradiated sample R2 (labeled with dose and time), and (b) unirradiated control sample LC2 (labeled with time).

The instrumentally corrected peak FWHM of the (00.2) peak in the longitudinal direction (±10°) is plotted as a function of dose and time for the irradiated and control samples, respectively, in Fig. 3. The data points shown for each sample are averages of the three volumes measured on each sample. The overall decrease in FWHM, calculated as the difference between the first and last data points, is 6.0 ± 1.1% (35 ± 6 μrad) up to 2935 kGy when averaged over all the irradiated samples. The average peak FWHM decrease in the (00.2) longitudinal direction for the control samples is 0 within experimental error (−0.33 ± 0.89%) for a time equivalent to irradiation up to 2935 kGy. For all the irradiated samples the peak widths decrease at a near linear rate up to about 330 kGy, beyond which the rate is reduced by an order of magnitude. A similar trend of decreasing peak width is also seen in the (00.4) longitudinal direction peaks, with an average decrease of 6.41 ± 0.67% (57 ± 6 μrad) for the irradiated samples (data shown in Supplementary Fig. S1).

The instrumentally corrected (00.2) and (00.4) peaks in the longitudinal direction were used in the Scherrer equation (Eq. (1)) to determine the RMS strain and the coherent size of the diffractors (the HAP platelets) in the sampled volume. First, the coherent HAP platelet size is plotted as a function of dose for the irradiated samples M1, M2, R1, and R2 in Fig. 4. The errors on these are the average of the standard deviation of the data points in LC1 and LC2, since these samples did not show any change with dose. A best fit analysis provides slopes, corresponding to the average change in the coherent size as a function of dose for the irradiated samples (M1, M2, R1, and R2), of $1.4 \times 10^{-3} \pm 5.4 \times 10^{-3}$ nm. Since the change in size is equal to 0 within error, the average size of the

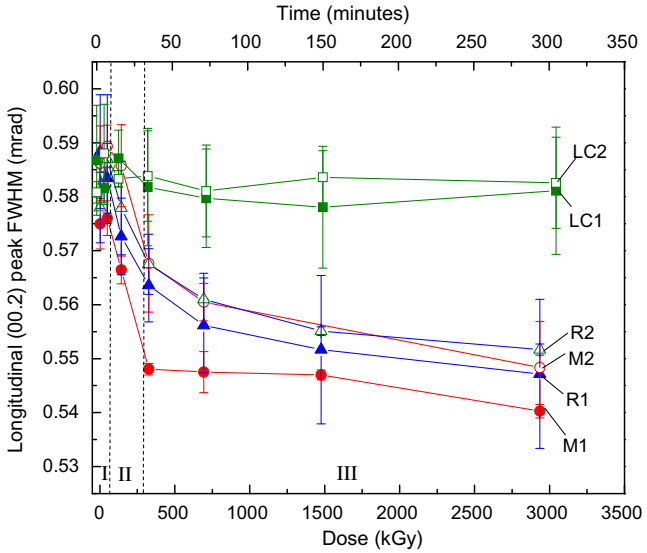

Fig. 3. Longitudinal HAP(00.2) peak full width at half maximum (FWHM) of the height as a function of irradiation dose without stress. Error bars are peak fitting errors propagated for the average of three measurements on each sample.

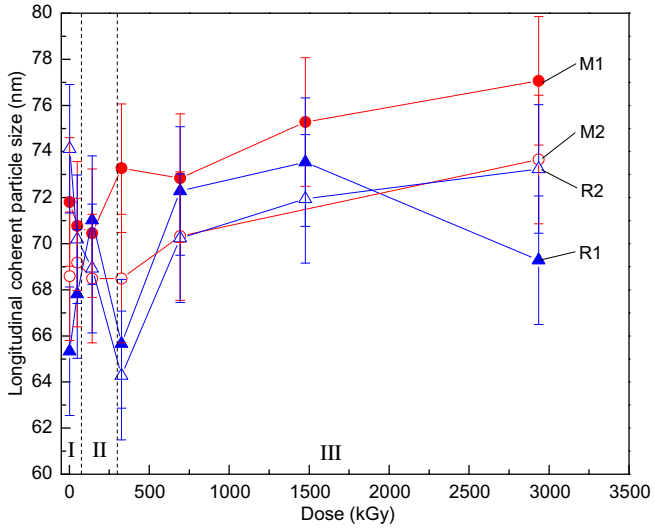

Fig. 4. Longitudinal coherent HAP crystallite size (Eq. (1)) as a function of irradiation dose without stress. Error bars are averages of standard deviations of points in the two control samples.

particles in all the samples for all doses was calculated as 70.5 ± 1.5 nm. This compares well with the values for LC1 (71.4 ± 5.4 nm) and LC2 (69.3 ± 5.4 nm). Second, the RMS strain in the particles is shown in Fig. 5 as a function of dose for samples M1, M2, R1, and R2, with error bars representing the average of the standard deviation of the data points in LC1 and LC2. The RMS strain shows a decreasing trend with dose for samples M1, M2, R1, and R2, albeit with sizeable scatter in the points, in Fig. 5. Initially there is little change in the RMS strain up to ~75 kGy (stage I), then there is a rapid decrease in the RMS strain up to 330 kGy (stage II), and finally the RMS strain saturates up to the maximum irradiation dose studied here (stage III). The average relative decrease in the RMS strains is 8.0 ± 3.3% (absolute value 470 ± 180 με) in samples M1, M2, R1, and R2up to a dose of 2935 kGy.

3.1.2. HAP lattice spacing

The HAP longitudinal (00.2) *d*-spacing was calculated from the peak centers of the pseudo-Voigt fit. In all the irradiated samples M1, M2, R1, and R2 the HAP *d*-spacing increases rapidly between ~75 and ~300 kGy (stage II), and then reaches a plateau (stage III), as shown in Fig. 6. An increase in the HAP *d*-spacing suggests a relaxation of the compressive lattice strain with dose. The average change in *d*-spacing, calculated as the difference between the first and last points in Fig. 6, in the irradiated samples is 0.03 ± 0.01% (0.001 ± 0.0003 Å) up to 2935 kGy.

3.2. Creep after irradiation

Samples were subjected to creep at an applied stress of −80 MPa after prior irradiation without stress, as described in Section 2.2.2. The doses varied from 0 to 7770 kGy. The HAP lattice strains are shown in Fig. 7a and b as a function of creep time for two samples, with prior doses of 47 (B1) and 422 (G1) kGy, respectively. The HAP lattice strains in the low irradiation sample B1 increase as a function of time, whereas those in the highly irradiated sample G1 decrease as a function of time. The HAP elastic strain rates were determined as a linear best fit of the data, as shown in Fig. 7a and b. This slope corresponds to the rate at which elastic strains are accumulated in or shed from the HAP phase as the surrounding protein matrix creeps. Fig. 8 shows the HAP elastic strain rates for the samples at all doses. At low doses, up to ~75 kGy, the slopes are negative (i.e. compressive strains increase with time) and constant (stage I). From ~75 kGy (start of stage II) to ~115 kGy the slopes remain negative, indicating load accumulation in the HAP phase during creep, but the value of the slopes increases towards 0. Beyond this dose the slopes become positive and continue to increase (i.e. compressive strains decrease with time), indicating load shedding by the HAP phase during creep. These positive slopes increase in magnitude up to a dose between 235 and 422 kGy (end of stage II), beyond which the slopes decrease (while remaining positive) and reach a plateau without changing further with increasing dose up to the highest dose studied (stage III).

4. Discussion

In the present study the effects of irradiation on various properties of unloaded samples (HAP *d*-spacing, HAP RMS strain, and HAP platelet size) and creep loaded samples (HAP strain accumulation/shedding) have been determined. Examination of the results indicates that many of these properties, HAP *d*-spacing, HAP RMS strain, and HAP strain evolution, exhibit three stages: stage I for doses below ~75 kGy, stage II for doses between ~75 and ~300 kGy, and stage III for doses between ~300 kGy and the highest value measured, 7771 kGy. The HAP platelet size appears to be dose invariant.

4.1. Properties affected by irradiation

4.1.1. Stage I – doses below ~75 kGy

The RMS strain and HAP *d*-spacing in the unloaded samples as well as the HAP elastic strain rate in the creeping samples show no significant changes in value between the lowest doses of ~2–5 and ~75 kGy (stage I, insets in Figs. 5, 6 and 8). This lack of variation indicates that below this dose there is no measureable change in the efficiency of load transfer from the collagen to HAP. This is indicative of a lack of change in the bone structure, collagen, or HAP properties, or in their interfacial behaviors. The near constant value of HAP *d*-spacing up to ~75 kGy is in agreement with previously published results that show little change in HAP residual strains up to ~75 kGy [10].

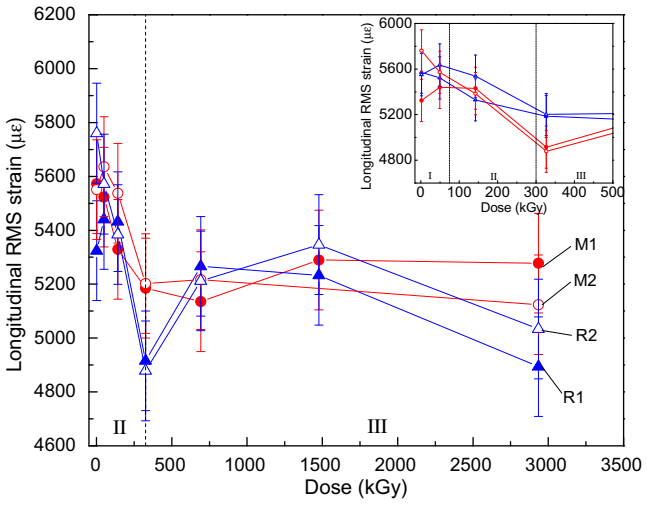

Fig. 5. Longitudinal RMS strain in HAP (Eq. (1)) as a function of irradiation dose without stress. Error bars are averages of standard deviations of points in the two control samples.

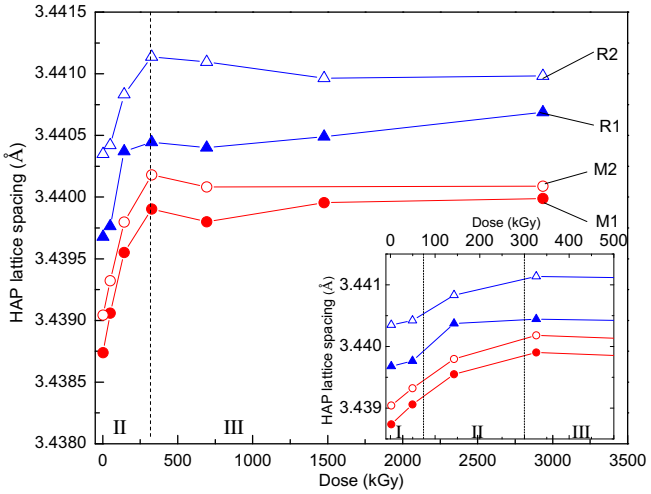

Fig. 6. Longitudinal HAP lattice *d*-spacing as a function of irradiation dose without stress.

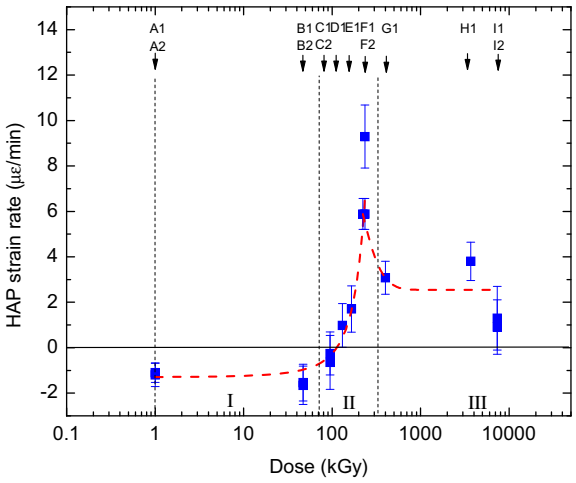

Fig. 8. HAP elastic strain rate during creep as a function of prior irradiation dose. Error bars are least squares linear fitting of the strain vs. time data for the individual samples.

4.1.2. Stage II – doses between ~75 and ~300 kGy

During stage II (~75–300 kGy) there are significant changes in the HAP *d*-spacing and RMS strain in unloaded samples, and the HAP elastic strain rates during creep. The HAP *d*-spacing of the unloaded samples, which is proportional to the residual strain, shows a rapid increase during stage II (Fig. 6), representing an increasingly tensile residual strain, while the RMS strain decreases (Fig. 5). Similarly, the HAP strain rates also increase during stage II, from a negative value (compressive load accumulation) to a positive value (load shedding) (Fig. 8). It has been hypothesized in the literature [9,10] that both a drop in residual strain and a decrease in compressive elastic strain accumulation rates due to irradiation is caused by damage at the HAP–collagen interface as a result of radiation-induced bond decarboxylation, the latter having been measured by Fourier transform infrared spectroscopy [34]: as the calcium-mediated carboxyl bonds between HAP and collagen are removed due to irradiation the interface is weakened, resulting in a decreased ability to transfer load from collagen to HAP.

In the case of unloaded samples the HAP is in a state of compressive residual strain, as also found in previous studies on bone employing X-ray diffraction techniques [10,20,21]. It is likely that compressive residual strain is formed during HAP platelet growth in constrained collagen matrix gaps and enforced by the collagen matrix. However, as the interfacial bonds are destroyed by irradiation the collagen becomes less able to sustain the load on the HAP platelets. As a result the strained HAP platelets relax and their *d*-spacing increases, as seen in Fig. 6.

This increase in *d*-spacing in the HAP platelets is accompanied by a decrease in their RMS strain (Fig. 5). The RMS strain, which represents the range of strains within the HAP platelets being sampled, is a measure of the distribution of strains between or within individual platelets. Therefore, a decrease in RMS strain indicates that the width of the distribution of strains between or within the platelets has narrowed. Examination of the intensity peaks reported in Fig. 2b shows an asymmetrical decrease in FWHM towards larger *d*-spacings, resulting in a narrower range of measured strains at higher doses. This suggests that relaxation preferentially occurs for those HAP unit cells which are initially under the most strain, i.e. those with the smallest *d*-spacings. Those unit cells with lower initial strains show little or no change with irradiation. This indicates that the HAP platelets (or regions within the platelets) that are under the highest residual strain are those most capable of relaxing as a result of irradiation damage, as expected given their higher elastic stored energy.

For the creep loaded samples the elastic strain rates during stage II pass from negative to positive values at ~115 kGy (Fig. 8). The HAP elastic strain rates of bone samples under creep represent a balance between (i) load accumulation by transfer from the collagen to the HAP due to interfacial shear stresses and (ii) load shedding from HAP to collagen due to interfacial damage, starting from the strain state in the HAP created after the initial loading of the sample from the unloaded state to the final creep load. In Fig. 8 the HAP elastic creep rates are initially negative, indicating that the collagen is transferring further compressive loads to HAP during creep (beyond those carried when both HAP and collagen deform elastically during initial loading of the sample), as would be expected in a composite system with a strong HAP–collagen interface [33]. However, as irradiation damages the HAP–collagen interface the efficiency of compressive load transfer from collagen to HAP during creep is decreased. This is initially visible as a decrease in the magnitude of the (negative) HAP strain rates. At ~115 kGy the magnitudes of the loads (i) transferred to HAP by the creeping collagen and (ii) shed back to collagen by HAP are equal, resulting in no net strain accumulation as creep proceeds (zero HAP strain rate). Beyond 115 kGy the HAP elastic

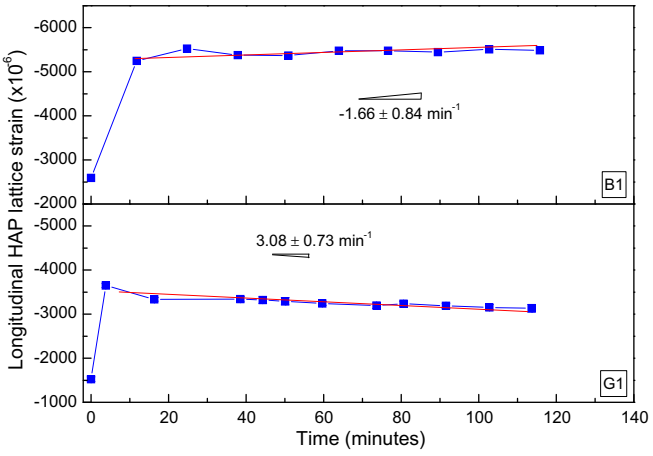

Fig. 7. HAP elastic strain vs. time curves for creep samples B1 (47 kGy prior dose) and G1 (522 kGy prior dose) showing the change in the sign of the slope (strain rate) from negative to positive with irradiation dose.

strain rates become positive, indicating that HAP is shedding some of the load accumulated during initial loading of the sample back to collagen as the latter creeps around it. This behavior is consistent with an increase in interfacial damage and collagen sliding as a higher dose is accumulated.

4.1.3. Stage III – doses above ~300 kGy

Above ~300 kGy and up to the highest dose of 7771 kGy the RMS strain and *d*-spacing of HAP in the unloaded samples reach a plateau (Figs. 5 and 6), which is consistent with saturation of interfacial damage due to irradiation. While in stage II increasing irradiation leads to a greater number of bonds being destroyed, the damage eventually reaches a plateau in stage III, when all of the non-reversible bonds are broken. This point is reached near 300 kGy for the conditions presented here. The remaining residual strain would result from the remaining hydrogen and Van der Waal forces present at the interface.

In stage III a plateau of HAP compressive strain shedding at 6–8 $\mu\varepsilon\ min^{-1}$ (which is the maximum strain rate reached at the end of stage II (Fig. 8)) would be expected in a situation where the HAP–collagen interface was fully damaged. However, the HAP strain rate drops by a factor of 2–4 between stages II and III (Fig. 8), i.e. HAP sheds load to collagen during creep less readily at very high doses, which cannot be explained by the damage hypothesis. This behavior could be explained by irradiation-induced cross-linking of the collagen matrix at doses around 300 kGy. Cross-linking between the collagen molecules has been suggested as a possible damage mechanism during irradiation [5,6,29,38,39]. An increase in the number of enzymatic and non-enzymatic cross-links with irradiation and aging limits the ability of collagen molecules to slide, stiffening and strengthening the matrix [6,40–42]. In the case of creep of previously irradiated bone the high collagen cross-linking may in fact serve to constrain the HAP platelets. In a finite element modeling study by the authors [9] unloading of HAP during creep of highly irradiated bone and dentin could be achieved if the collagen molecules were able to debond and slide past the platelets. However, without collagen sliding the shear stresses on the HAP–collagen interface would be decreased and the interfacial damage limited. If the cross-linking were to reach a critical level at values around 300 kGy it is possible that the stiffer collagen matrix could reduce the tendency for the HAP phase to shed load, thus explaining the decrease in HAP elastic strain rate at high doses.

Collagen cross-linking could also explain the behavior of the unloaded samples. When the matrix is compliant the HAP platelets can more easily relax, deforming the surrounding viscoelastic collagen. However, with a stiffer cross-linked matrix it becomes more difficult for the HAP platelets to displace the collagen, constraining the platelet more efficiently and stopping full HAP relaxation earlier, resulting in the plateau behavior visible in Fig. 8. Although beyond the scope of this paper, Raman measurements should be done on irradiated bone samples to confirm the presence of collagen–collagen crosslinking.

4.2. Irradiation invariant properties

The best fit average value of 70.5 ± 1.5 nm for longitudinal HAP size (Fig. 4) is in excellent agreement with the value of 67 nm previously measured in bovine bone [9], but significantly larger than the 41–44 nm value found in canine fibula [20] using the same synchrotron X-ray method in both cases. No change in the coherent longitudinal HAP size was observed with dose, which is unsurprising since increased biomineralization would not be expected to occur with increased radiation dose in an extracted bone. However, if high energy radiation were to cause small amounts of physically induced mineralization it would be difficult to detect it with this technique. If a single unit cell of mineralizing material (HAP) was added to each side of the longitudinal dimension of the HAP platelets (c = 6.884 Å) it would represent a change in longitudinal length of <2%. This is significantly less than the scatter of the measurements, which represent about 4% of the average observed size of the diffractors. A minimum of five unit cells would have to be added to each longitudinal surface to distinguish a change in size. Evaluating the smaller transverse (3 1 0) direction of the HAP platelets gives an average platelet dimension of 8.3 ± 1.3 nm, which does not vary significantly with dose (Supplementary Fig. S2). This value may be smaller than the actual value due to the assumption that the RMS strain in this direction is 0 in Eq. (1). This smaller dimension should be more sensitive to size changes, however, the small number of (3 1 0) crystallites oriented in this direction results in highly scattered data.

5. Conclusions

Synchrotron X-ray diffraction was used to measure the elastic strain state of the HAP mineral phase, the *d*-spacing and RMS strain in unloaded samples and the elastic strain rate (strain vs. time) in compressive creep experiments in bovine bone. These three HAP strain measurements exhibit a three stage behavior (threshold, HAP–collagen interface damage, and plateau) with increasing X-ray dose.

- In stage I (below ~75 kGy, threshold stage) none of the three HAP strain measurements show significant changes in value, indicating that the HAP strain state under unloaded and creep loaded conditions is initially unaffected by irradiation.
- In stage II (between ~75 and ~300 kGy, damage stage) the HAP *d*-spacing increases and the RMS strain decreases with increasing dose in load-free samples. This is consistent with a release of compressive residual strains in the HAP platelets due to interfacial damage. The asymmetrical decrease in the FWHM of the (0 0 .2) diffraction peaks indicates that those HAP unit cells under the highest initial residual strains are most able to relax as a result of irradiation.
- In stage II under creep loading conditions the HAP elastic strain rate decreases with increasing dose from negative (i.e. HAP accumulates load from the creeping collagen matrix) to positive (i.e. HAP sheds load to the creeping matrix). Increasing interfacial damage can again be invoked to explain this trend.
- In stage III (beyond ~300 kGy, plateau stage, explored up to 7771 kGy) all three HAP strain measurements reach a plateau. The *d*-spacing and RMS strain attain a constant level at ~300 kGy, while the HAP elastic strain rate remains in load shedding mode, but less so than at the end of stage II. These observations are consistent with damage saturation and/or a stiffening of the matrix due to collagen cross-linking.

Our observations indicate that it is essential to consider the effects that X-ray irradiation has on the mechanical properties of bone, and establish doses of ~75 and ~300 kGy as critical values for threshold and plateau values for mechanical response, respectively. Given that reliable wide-angle (and small-angle) scattering patterns can be obtained at ~1 kGy by the method presented, experiments should be planned to keep a given sample volume below these values through sample translation and/or limiting the maximum number of patterns/amount of data obtained.

Acknowledgements

Use of the Advanced Photon Source (APS) was supported by the US Department of Energy, Office of Science, Office of Basic Energy

Sciences, under contract no. DE-AC02-06CH11357. This research was performed at station 1-ID of the XOR-APS. Partial funding was provided to A.C.D.B. by a National Defense Science and Engineering Graduate Fellowship from the Department of Defense and National Science Foundation and a National Science Foundation Graduate Fellowship from the National Science Foundation. The authors thank Dr. Dean R. Haeffner (APS) for numerous useful discussions throughout this work. They also acknowledge Dr. Yu-Chen Karen Chen (Northwestern University) for her help with the experiments at the APS.

Appendix A. Figures with essential colour discrimination

Certain figures in this article, particularly Figs. 1–8, are difficult to interpret in black and white. The full colour images can be found in the on-line version, at http://dx.doi.org/10.1016/j.actbio.2012.07.046).

Appendix B. Supplementary data

Supplementary data associated with this article can be found, in the online version, at http://dx.doi.org/10.1016/j.actbio.2012.07.046.

References

[1] Kruzic JJ, Nalla RK, Kinney JH, Ritchie RO. Crack blunting, crack bridging and resistance-curve fracture mechanics in dentin: effect of hydration. Biomaterials 2003;24:5209–21.
[2] Ritchie RO. The conflicts between strength and toughness. Nat Mater 2011;10:817–22.
[3] Ritchie RO, Buehler MJ, Hansman PK. Plasticity and toughness in bone. Phys Today 2009;3:41–7.
[4] Vashisth D. Rising crack-growth-resistance behavior in cortical bone: implications for toughness measurements. J Biomech 2004;37:943–6.
[5] Barth HD, Launey ME, MacDowell AA, Ager JW, Ritchie RO. On the effect of X-ray irradiation on the deformation and fracture behavior of human cortical bone. Bone 2010;46:1475–85.
[6] Barth HD, Zimmermann EA, Schaible E, Tang SY, Alliston T, Ritchie RO. Characterization of the effects of X-ray irradiation on the hierarchical structure and mechanical properties of human cortical bone. Biomaterials 2011;32:8892–904.
[7] Cornu O, Banse X, Docquier PL, Luyckx S, Delloye C. Effect of freeze-drying and gamma irradiation on the mechanical properties of human cancellous bone. J Orthop Res 2000;18:426–31.
[8] Currey JD, Foreman J, Laketic I, Mitchell J, Pegg DE, Reilly GC. Effects of ionizing radiation on the mechanical properties of human bone. J Orthop Res 1997;15:111–7.
[9] Deymier-Black AC, Singhal A, Yuan F, Almer JD, Brinson LC, Dunand DC. High-energy X-ray diffraction study of creep mechanisms in bone and dentin. Bone; accepted for publication.
[10] Singhal A, Deymier-Black AC, Almer JD, Dunand DC. Effect of high-energy X-ray doses on bone elastic properties and residual strains. J Mech Behav Biomed Mater 2011;4:1774–86.
[11] Alwood JS, Yumoto K, Mojarrab R, Limoli CL, Almeida EAC, Searby ND, et al. Heavy ion irradiation and unloading effects on mouse lumbar vertebral microarchitecture, mechanical properties and tissue stresses. Bone 2010;47:248–55.
[12] Hamilton SA, Pecaut MJ, Gridley DS, Travis ND, Bandstra ER, Willey JS, et al. A murine model for bone loss from therapeutic and space-relevant sources of radiation. J Appl Physiol 2006;101:789–93.
[13] Franzel W, Gerelach R. The irradiation action on human dental tissue by X-rays and electrons-a nanoindenter study. Z Med Phys 2009;19:5–10.
[14] Kielbassa AM, Hinkelbein W, Hellwig E, Meyer-Luckel H. Radiation-related damage to dentition. Lancet Oncol 2006;7:326–35.
[15] Thariat J, De Mones E, Darcourt V, Poissonnet G, Dassonville O, Savoldelli C, et al. Teeth and irradiation in head and neck cancer. Cancer Radiother 2010;14:128–36.
[16] Nguyen H, Morgan DAF, Forwood MR. Sterilization of allograft bone: effects of gamma irradiation on allograft biology and biomechanics. Cell Tissue Bank 2007;8:93–105.
[17] Nyman JS, Reyes M, Wang X. Effect of ultrastructural changes on the toughness of bone. Micron 2005;36:566–82.
[18] Akhtar R, Daymond MR, Almer JD, Mummery PM. Load transfer in bovine plexiform bone determined by synchrotron X-ray diffraction. J Mater Res 2008;23:543–50.
[19] Akhtar R, Daymond MR, Almer JD, Mummery PM. Elastic strains in antler trabecular bone determined by synchrotron X-ray diffraction. Acta Biomater 2008;4:1677–87.
[20] Almer JD, Stock SR. Internal strains and stresses measured in cortical bone via high-energy X-radiation. J Struct Biol 2005;152:14–27.
[21] Almer JD, Stock SR. Micromechanical responses of mineral and collagen phases in bone. J Struct Biol 2007;157:365–70.
[22] Deymier-Black AC, Almer JD, Stock SR, Haeffner DR, Dunand DC. Synchrotron X-ray diffraction study of load partitioning during elastic deformation of bovine dentin. Acta Biomater 2010;6:2172–80.
[23] Gupta HS, Seto J, Wagermaier W, Zaslansky P, Boesecke P, Fratzl P. Cooperative deformation of mineral and collagen in bone at the nanoscale. Proc Natl Acad Sci USA 2006;103:17741–6.
[24] Gupta HS, Wagermaier W, Zickler GA, Hartmann J, Funari SS, Roschger P, et al. Fibrillar level fracture in bone beyond the yield point. Int J Fract 2006;139:425–36.
[25] Gupta HS, Wagermaier W, Zickler GA, Raz-Ben Aroush D, Funari SS, Roschger P, et al. Nanoscale deformation mechanisms in bone. Nano Lett 2005;5:2108–11.
[26] Stock SR, De Carlo F, Almer JD. High energy X-ray scattering tomography applied to bone. J Struct Biol 2008;161:144–50.
[27] Bouxsein ML, Boyd SK, Christiansen BA, Guldberg RE, Jepsen KJ, Muller R. Guidelines for assessment of bone microstructure in rodents using micro-computed tomography. J Bone Mineral Res 2010;25:1468–86.
[28] Brauer DS, Saeki K, Hilton JF, Marshall GW, Marshall SJ. Effect of sterilization by gamma radiation on nano-mechanical properties of teeth. Dent Mater 2008;24:1137–40.
[29] Akkus O, Belaney RM, Das P. Free radical scavenging alleviates the biomechanical impairment of gamma radiation sterilized bone tissue. J Orthop Res 2005;23:838–45.
[30] Akhtar R, Daymond MR, Almer JD, Mummery PM. Lattice strains and load partitioning in bovine trabecular bone. Acta Biomater 2011;7:716–23.
[31] Deymier-Black AC, Almer JD, Stock SR, Dunand DC. Variability in the elastic properties of bovine dentin at multiple length scales. J Mech Behav Biomed Mater 2012;5:71–81.
[32] Deymier-Black AC, Almer JD, Haeffner DR, Dunand DC. Effect of freeze–thaw cycles on load transfer between the biomineral and collagen phases in bovine dentin. Mater Sci Eng C 2011;31:1423–8.
[33] Deymier-Black AC, Yuan F, Singhal A, Almer JD, Brinson LC, Dunand DC. Evolution of load transfer between hydroxyapatite and collagen during creep deformation of bone. Acta Biomater 2012;8:253–61.
[34] Hubner W, Blume A, Pushjakova R, Dekhtyar Y, Hein HJ. The influence of X-ray radiation on the mineral/organic matrix interaction of bone tissue: an FT-IR microscopic investigation. Int J Artif Organs 2005;28:66–73.
[35] Hammersley AP. FIT2D V9.129 Reference Manual V3.1. Grenoble, France: European Synchrotron Radiation Facility; 1998.
[36] Noyan IC, Cohen JB. Residual stress: measurement by diffraction and interpretation. New York: Springer-Verlag; 1987.
[37] Singhal A, Almer JD, Haeffner DR, Dunand DC. Load partitioning between mineral and protein phases during compressive deformation of bone. Acta Bio 2012;8:2747–58.
[38] Akkus O. Elastic deformation of mineralized collagen fibrils: an equivalent inclusion based composite model. J Biomech Eng 2005;127:383–90.
[39] Dziedzic-Goclawska A, Kaminski A, Uhrynowska-Tyszkiewicz I, Stachowicz W. Irradiation as a safety procedure in tissue banking. Cell Tissue Bank 2005;6:201–19.
[40] Bailey AJ. Molecular mechanisms of ageing in connective tissues. Mech Ageing Dev 2001;122:735–55.
[41] Bailey AJ, Rhodes DN, Cater CW. Irradiation-induced crosslinking of collagen. Radiat Res 1964;22:606–21.
[42] Bailey AJ, Tromans WJ. Effects of ionizing radiation on the ultrastructure of collagen fibrils. Radiat Res 1964;23:145–55.